A NEW METHOD FOR STEREO- CAMERAS SELF-CALIBRATION IN SCHEIMPFLUG CONDITION

S. Hamrouni[1], H. Louhichi[1], H. Ben Aissia[1], M. Elhajem[2]

[1]Unité de Métrologie en Mécanique des Fluides et Thermique, Ecole Nationale d'Ingénieurs, Monastir, 5000, Tunisie.
[2]Laboratoire de Mecanique des Fluides et Acoustique (LMFA), INSA de Lyon, Université de Lyon, France

[H]: Tel.: + 21673500514; Fax: + 21673500514; Email: hamrouni_salha@yahoo.fr

KEYWORDS:
Stereo PIV, Self-calibration, Scheimpflug condition, macro-particle

ABSTRACT: The calibration of a Scheimpflug SPIV device is actually achieved in two steps from a bundle adjustment technique. The SPIV recording system is first calibrated by imaging the planar target at different location and then the laser plane equation is obtained from a geometrical optimization. The misalignments between the laser sheet plane and the calibration plane always remains significant. In this paper we demonstrated How to calibrate a camera model directly into the laser sheet. A new scheimpflug model is applied to calibrate a cameras system. This new approach is based on the use of a target formed by spherical macro-particle. Experimental results on real data show the relevance of the proposed method.

1 Introduction

The Scheimpflug condition enables to focus a video-camera when oblique viewing at low aperture number. It is used in Stereoscopic Particle Image Velocimetry (SPIV) for measuring the three-dimensional velocity field in a section of a flow [1][2]. This condition is performed by tilting the sensor (or the lens) such that the object plane, the lens plane and the image plane intersect in a common line (figure 1). The three velocity components are reconstructed from mapping functions. One mapping function per camera is used to relate any 3D location to its image. The parameters of each mapping function are recovered at the calibration stage.

A precise target is usually placed in a reference plane for the calibration of SPIV cameras. If the target is a planar one, it has to be accurately moved to different locations in depth. Other multi-level targets, on which different z-positions are present, are available for the special case of SPIV calibration. In [3], accurate axial displacements are required by the calibration protocol. All these calibration methods may be unstable if the positioning of the target is not accurate enough. Besides a method using a single image of a dot grid target was proposed in [4] but given the focal length and sensor pixel pitches of the PIV camera.

Self-calibration does not use such additional accurate information on the recording system. A non linear least mean square procedure allows the (bundle) adjustment of the vector of the calibration parameters after their rough initialization. The coordinates of the calibration points are included in this vector. Such an approach can present two practical advantages [5]. Firstly it does not require metrological calibration targets so that calibration targets can be home-made and easily adjusted to be studied field of view. Secondly it relaxes the constraint of an accurate positioning of the calibration plate by a controlled translation stage device. The SPIV recording system is first calibrated by imaging the planar target at different location [6] and then the laser plane equation is obtained from a geometrical optimization.

Despite these advantages, the misalignments between the laser sheet plane and the calibration plane always remains significant [7].

The aim of this paper is to combine this two mentioned steps in one level using a new camera model in scheimpflug condition. It consists of making the calibration directly into the laser sheet. The new camera model in scheimpflug condition is described in section 2. In section 3, we present the technique of Feature points detection. The homography between image plane when imaging the laser plane is determined in section 4. Experimental results on real data show how the relevance of the proposed method.

2 Scheimpflug camera model.

2.1. Self-calibration from multiple images.

The Scheimpflug camera model is based on the pin-hole assumption. In the latter, the image plane is parallel to the lens plane but in the Scheimpflug camera model the image plane is tilted respect to the lens plane as can be seen in the Fig. 1. The conditions of the α angle (twisting of the lens plane around the X_{cam} axis see (3)) and the laser plane should be the following : $\frac{x_0}{z_0} = \frac{x_i}{z_i}$ so that $\frac{1}{d_0} + \frac{1}{d_i} = \frac{1}{f}$,(see Fig. 1)

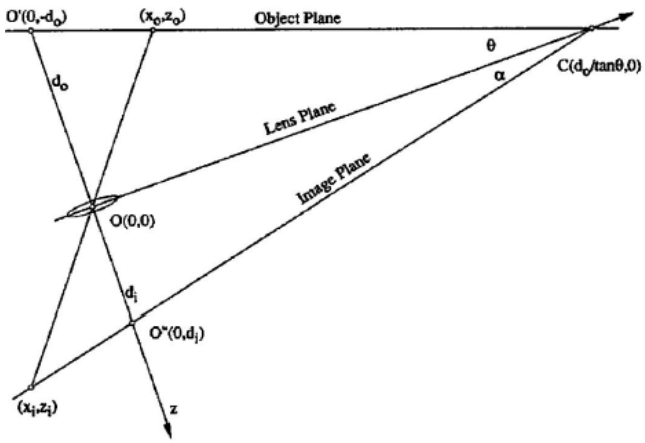

Fig. 1. Coordinate systems in Scheimpflug condition .

In the pinhole camera model, the extrinsic parameters are the rotation matrix R and the translation vector T to change from the world plane to the camera plane, and the intrinsic parameters correspond to the focal length multiplied by the pixel to millimeter factors (F_x,F_y), intersection of the optical axis with the image plane (C_x ,C_y) and the distortion parameters (equation (1)), where s is any real number different from zero. See later on the radial distortion definition.

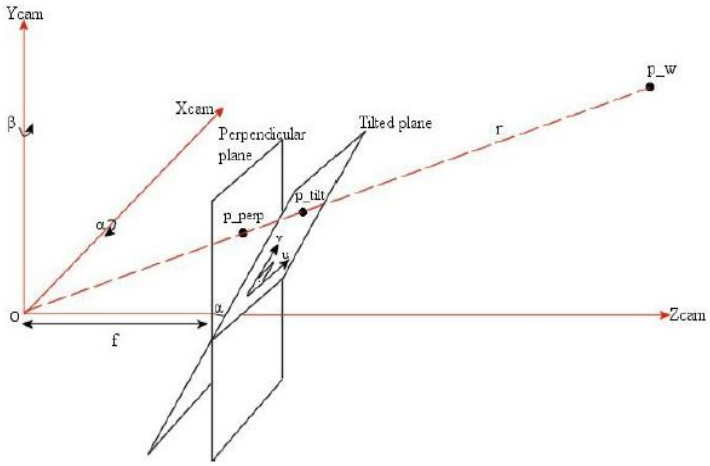

Fig. 2. Intersection of the point in the real world in the tilted plane and in the perpendicular plane taken from[14].

$$\begin{pmatrix} s.x_{pix} \\ s.y_{pix} \\ s \end{pmatrix} = \begin{pmatrix} F_x & 0 & c_x \\ 0 & F_y & c_y \\ 0 & 0 & 1 \end{pmatrix} \left[R \begin{pmatrix} x_w \\ y_w \\ z_w \end{pmatrix} + T \right] \tag{1}$$

To this pinhole model equation (1), two extra parameters (α,β) are added. α is the between Y_{cam} axis and v vector (which can be arbitrarily chosen as the vertical direction of the tilted CCD plane), and β is the angle between the u vector (which can be arbitrarily chosen as the horizontal direction of the CCD tilted plane) and the vector X_{cam}, see Fig. 2.

The origins of the tilted and the perpendicular plane are the same, as the perpendicular plane can be arbitrarily placed. Cameras under Scheimpflug condition have been used in Steroscopic Particle Image Velocimetry (SPIV), but in this works [8], [9], they consider a rotation matrix for small angles between the perpendicular plane and the tilted plane, resulting in three degrees of freedom when only two degrees are needed. In [10] the rotation angles are small because they corrected the tilted lens of the camera due to the weight on the lens. Another interesting work, [11], considers the inclination of the sensor as an additional distortion, the radial distortion being the same as in Brown model [12]. They change the tangential distortion adding a rotation matrix. This is only useful for small angles. Finally [13] develops a system of eleven linear equations in which only one Scheimpflug angle is included.

In order to transform points from the tilted plane to the perpendicular plane (Fig. 2), we have the following scenario. The point $p_w = (x_w, y_w, z_w)'$ is a point in the world and r is a straight line which goes from the point p to the optical center o. This line crosses the tilted image plane and the perpendicular image plane. The vector u is defined as $u = (\cos\beta, 0, \sin\beta)'$. That vector u lies in the plane X_{cam}, Z_{cam}. The other vector v is perpendicular to the u and has an α angle with the Y_{cam} vector. Hence the vector $v = (-\sin\alpha * \sin\beta, \cos\alpha, \sin\alpha * \cos\beta)$. It is verified that $u' * v = 0$, (where u' is the transpose to the vector u in matrix notation). The following all transposed vectors are noted the same way.

The Equation of the line is:

$$\text{r: } \lambda * p_w = \lambda * (x_w, y_w, z_w)' \tag{2}$$

The projected point p_{per} in the perpendicular plane at a distance f is:

$$p_{per} = (p_{perx}, p_{pery}, f)' \tag{3}$$

In [14], Legarda has defined the projected point p_{tilt} in the tilted plane at a distance f as following:

$$p_{tilt} = (0,0,f)' + p_{tiltx} * u + p_{tilty} * v \tag{4}$$

From (3), (4) the straight line passing though the point p_{tilt} intersects in the perpendicular plane:

$$\lambda * ((0,0,f)' + p_{tiltx} * u + p_{tilty} * v) = (p_{perx}, p_{pery}, f)' \tag{5}$$

Resulting:

$$\lambda = f / (f + p_{tiltx} * \sin\beta + p_{tilty} * \sin\alpha * \cos\beta) \tag{6}$$

Finally we obtain the point in the perpendicular plane p_{per} the tilted one p_{tilt}:

$$(p_{perx}, p_{pery})' = \lambda * (p_{tiltx} * (\cos\beta, 0)' + p_{tilty} * (\sin\alpha * \cos\beta, \cos\alpha)') \tag{7}$$

To do just the opposite transformation, i.e, to calculate the point in the tilted plane using the information in the perpendicular plane, the result can be easily derived:

$$\begin{aligned} p_{tiltx} &= \lambda_1 * \left(\frac{p_{perx}}{\cos\beta} + p_{pery} * \tan\alpha * \tan\beta\right) \\ p_{tilty} &= \lambda_1 * \frac{p_{pery}}{\cos\alpha} \end{aligned} \tag{10}$$

Where λ_1 is defined as:

$$\lambda_1 = f \Big/ \left(f - p_{perx} * \tan\beta - p_{pery} * \frac{\tan\alpha}{\cos\beta}\right) \tag{11}$$

In order to consider the lens distortion, we transform first the observed points (in the tilted plane) to the perpendicular one. For these transformed points, in the perpendicular plane, only radial distortion[12] have to be applied due to the radial symmetry of the lenses respect to their optical axis.

$$\begin{aligned} p_{per}x_{dist} &= p_{per}x_{und} + \delta_{p_{per}x_{und}}(p_{per}x, p_{per}y) \\ p_{per}y_{dist} &= p_{per}y_{und} + \delta_{p_{per}y_{und}}(p_{per}x, p_{per}y) \end{aligned} \tag{12}$$

$$\begin{aligned} \delta_{p_{per}x_{und}}(p_{per}x, p_{per}y) &= \Delta_{p_{per}x}(k_1 r^2 + k_2 r^4 + k_3 r^6) \\ \delta_{p_{per}y_{und}}(p_{per}x, p_{per}y) &= \Delta_{p_{per}y}(k_1 r^2 + k_2 r^4 + k_3 r^6) \end{aligned} \tag{13}$$

r is the distance from the pixel to the principal point of the image, $\Delta_{p_{per}x} = x_p - x_0$, $\Delta_{p_{per}y} = y_p - y_0$. The radial distortion coefficients are: k_1, k_2, k_3, where $r^2 = \Delta x^2 + \Delta y^2$.

3 Feature points detection

We propose to use points tangent to dots and their projections in images to perform calibration [15]. The tangency points will be determined by selecting bi-tangents i.e. tangents commons to a pair of dots. In the case of two separated ellipses, there exist four bi-tangents, two internal (LL,

RR). In this way, 6 intersections between bi-tangents can be added as invariant points to the 8 tangency points as shown in Fig.3. In order to get more feature points. For these points which does not require to mark dots, there is no offset due to the perspective projection.

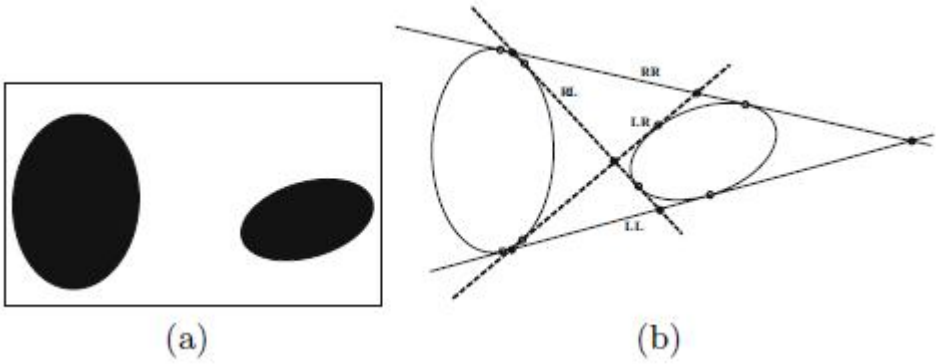

Fig. 3. Bitangents and feature points extraction (a) Original image (b) Common tangents(solid lines: external tangents, dashed lines : internal tangents) and associated feature points (filled circles : tangent points, rings : bitangent intersection points.

To obtain this tangency points, the block diagram of the figure below summarizes the different step:

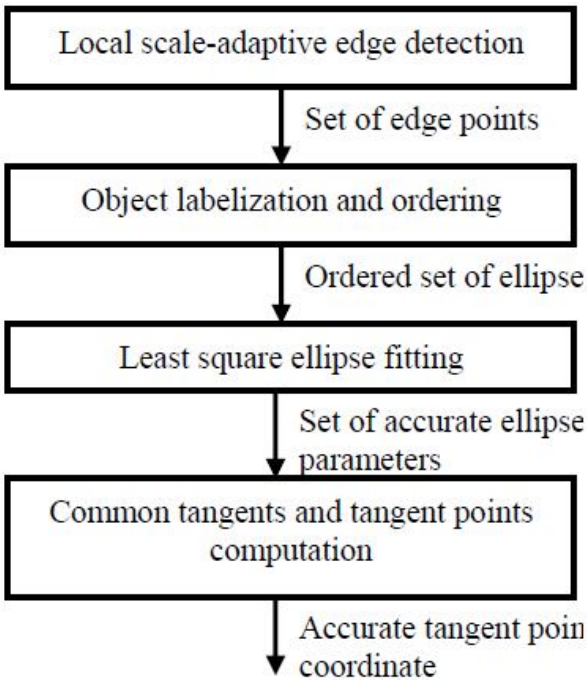

Fig. 4. Blok diagram of the tangency points approach

4 Laser plane equation

After calibration of the stereo system, the rigid transformation (R_s,t_s) from the second camera coordinate system to the first one for the i^{th} view is given by:

$$\begin{pmatrix} R_i^{(1)} & t_i^{(1)} \\ 0 & 1 \end{pmatrix} = \begin{pmatrix} R_h & t_h \\ 0 & 1 \end{pmatrix} \begin{pmatrix} R_i^{(2)} & t_i^{(2)} \\ 0 & 1 \end{pmatrix} \tag{14}$$

Let us assume that optical distortions are corrected. As the projections are perspective ones, there exists a pure homography transformation H between points $x^{(1)}$ (of pixel homogeneous coordinates $u^{(1)}$) and $x^{(2)}$ (of pixel homogeneous coordinates $u^{(2)}$) :

$$s\,u^{(2)} = H\,u^{(1)} \tag{15}$$

Where H is (3 × 3) matrix defined with only 3 unknown parameters and s is a scalar introduced in order to normalize the third component of $u^{(2)}$. In fact, the image $u^{(2)}$ is the image of the back projection of $u^{(1)}$ on the laser plane.

The laser plane being defined by the distance d from the first projection center and by the normal vector $n=(n_x,n_y,n_z)^T$, the homography H can be expressed as:

$$H = \begin{pmatrix} p_x^{(2)} & 0 & u_0^{(2)} & 0 \\ 0 & p_y^{(2)} & v_0^2 & 0 \\ 0 & 0 & 1 & 0 \end{pmatrix} \begin{pmatrix} R_h^T & -t_h^T \\ 0 & 1 \end{pmatrix} \begin{pmatrix} 1 & 0 & 0 & 1 \\ 0 & 1 & 0 & 0 \\ 0 & 0 & 1 & 0 \\ n_x/d & n_y/d & n_z/d & 0 \end{pmatrix} \begin{pmatrix} 1/p_x^{(1)} & 0 & -u_0^{(1)}/p_x^{(1)} \\ 0 & 1/p_y^{(1)} & -v_o^{(1)}/p_y^{(1)} \\ 0 & 0 & 1 \\ 0 & 0 & 1/p^{(1)} \end{pmatrix} \tag{16}$$

The purpose is to find the unknowns $(a,b,c)^T = \frac{1}{d}\,n$ which leads to the laser plane equation. The solution $(\tilde{a},\tilde{b},\tilde{c})^T$ can be estimated by minimizing the sum $\sum_{i=1}^{2mn} \varepsilon_i^T\,\varepsilon_i$ where ε_i is the deviation vector between measured position $u_i^{(2)}$ (corresponding to the i^{th} measured position $u_i^{(1)}$) and the current value $\frac{1}{s}H(a,b,c)u_i^{(1)}$.

5 Experimental results.

The method mentioned in section 2 for SPIV self-calibration has been applied on a pair of 1024 × 768 1/2" CCD cameras (Sony XC 700) mounted on the Scheimpflug devices. The CCD cameras were equipped with f=50mm lenses focused on the measurement plane with a distance of 500 mm and viewing it at 45°. This new method is applied using printed target and macro-particle into laser sheet.

5.1. Using printed target.

Five photographs of ellipses of printed target are recorded by each camera at different positions as shown in Fig. 5(a). The tangency points obtained using the method described in section 3 are illustrates in Fig. 5(b). The results of calibration are shown in table 1. As can be seen the use of bitangents allows accurate estimates: for example, the estimate of Scheimpflug tilt (theoretical values: $\alpha = 2.8°,\ \beta = 0°$) is $\alpha = 2.7° \pm 0.17°,\ \beta = 0.01° \pm 0.002°$. Once can notice a relative

deviation (inferior to 1%) of image distance p_x with respect to focal length f_x=8000 as the lens was separated from the CCD device for Scheimpflug tilt.

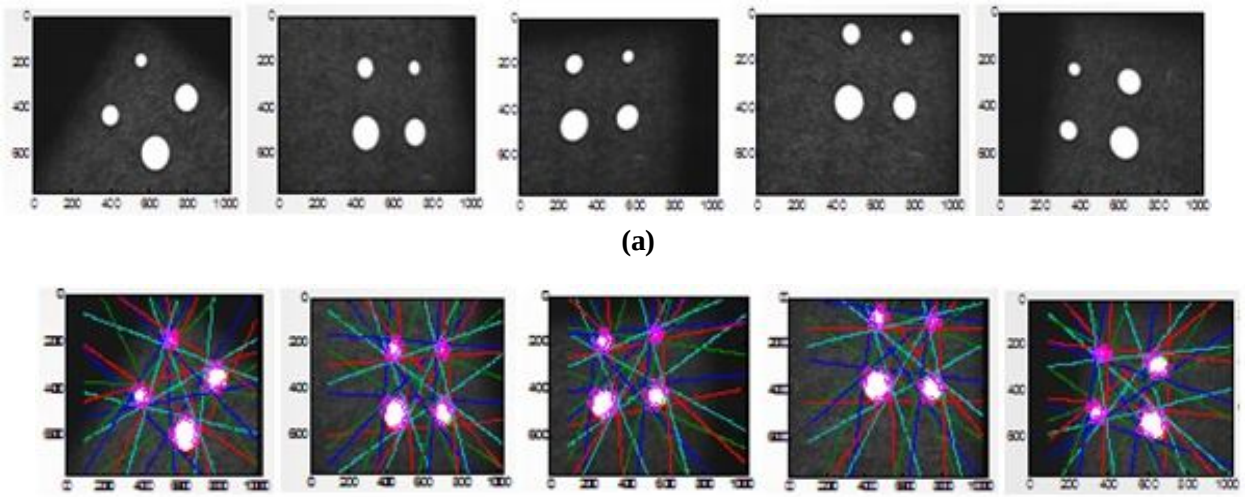

(a)

(b)

Fig. 5. **(a)** Photographs of ellipses target at different positions
(b) Bitangents and tangency points for ellipses at different positions

Intrinsic parameters	p_x (pixel)	p_y (pixel)	u_0 (pixel)	v_0(pixel)	a_1	a_2	a_3	α(degree)	β(degree)
	8067.52	8067.52	503.12	361.87	3.851	0.92	0.28	2.7	0,01
Standard deviation	0.807	0.807	0.63	0.38	0.390	0.041	0.03	0.17	0,0 02

Table 1. Results of self-calibration with printed target.

5.2. Using macro particle into laser sheet

We have keep the same cameras system. We have just replace the printed target by macro-particles in the laser plane. An Argon continue laser sheet (λb =488nm, λv = 514.5nm) with a maximum power of 7W. The laser plane was located in the depth of field of the cameras.

In these experiments, the target is a cross-sections of two 20-25 mm spherical soap bubbles filled with smoke were illuminated by laser sheet(about 1 mm thick). These Cross-sections marked the laser plane as two circular dots which can be imaged into large ellipses in image planes as shown in Fig. 6.

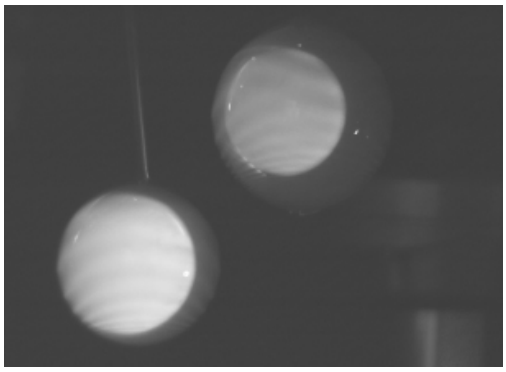

Fig. 6. test of two soap bubbles

In order to calibrate the system of cameras in Scheimpflug model, 5 views of the target were recorded by each camera. The points belonging to the bitangents of the two ellipses (Fig. 7) are computed according the algorithm given in section 3. The cameras were calibrated using the tangency points. For each camera, reliable results are obtained as shown in table 2.

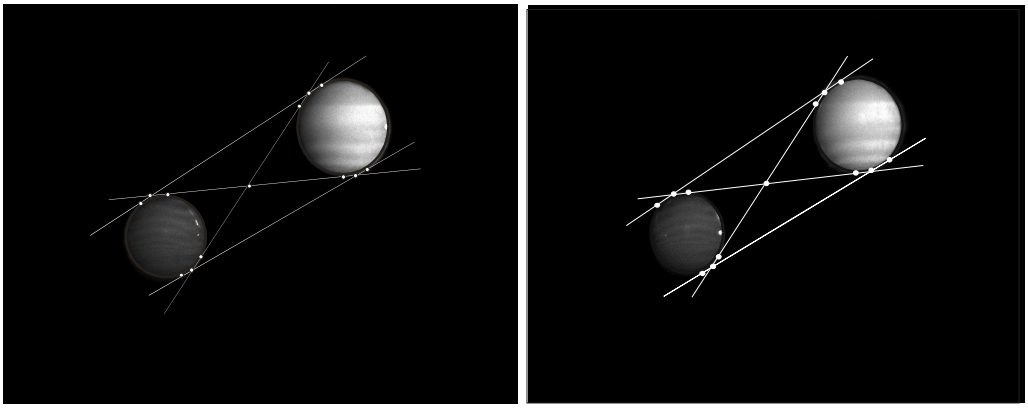

Fig. 7. Feature points belonging to the bitangents of the two ellipses

Optimal parameters of the right cameras			Optimal parameters of the left cameras		
Intrinsic parameters		σ	Intrinsic parameters		σ
u_0 (pixel)	518.13	0.41	u_0 (pixel)	513.35	0.37
v_0 (pixel)	379.28	0.23	v_0 (pixel)	381.10	0.42
f (pixel)	8011.33	0.17	f (pixel)	8010.92	0.19
α(degree)	2.79	0.34	α(degree)	2.79	0.33
β(degree)	0.02	0.0023	β(degree)	0.02	0.0021

Table 2. Results of Scheimpflug self-calibration using macro-particles.

A 6th view is recorded by each camera and used to find the laser equation. Table 3 shows the results of the laser plane equation using the homographic method. θ_1 is the angle under (*ox*), θ_2 is the angle under (*oy*), θ_3 is the angle under (*oz*).

Position of the laser plane			
θ_1	θ_2	θ_3	d
2.51	43.78	1.83	513.46

Table 3. Results of the laser plane parameters

6. Conclusion

Self-calibration of Scheimpflug cameras allows easy calibration by viewing a target at different locations in the depth of field. The cameras parameters are recovered from the bundle adjustment technique using the new scheimpflug model proposed by Legarda[14]. The laser equation is obtained from a geometrical optimization. The misalignments between the laser sheet plane and the calibration plane always remains significant. We have proposed a method to combine the two steps in one level. However, the cameras parameters and the parameters of the laser plane can be obtained simultaneously. The target can be positioned directly in the laser sheet. This technique allows to getting rid of the problem of correcting misalignment between the calibration plane and the laser plane.

Our approach is based on the use of a target formed by a *macro-particle* which can be entirely seen in the laser plane. The feature points are determined using the tangency points technique. Such a procedure leads to detect a fifteen feature points at a subpixel precision. The obtained experimental results confirm the relevance of the proposed method.

References

[1] Hinsch K D, Hinrichs H, Roshop A, Dreesen F 1993 Holograpic and stereoscopic advance in 3DPIV. Holographic Particle Image Velocimetry. *Proc. of Fluids Engineering Division, AmericanSociety of mechnical Engineers.* E P Rood (Washington, DC:ASME), (148), 33-6.

[2] Prasad A K, Jens K 1995 Scheimpflug stereocamera for particle image velocimetry in liquid flow. *Applied Optical* (34**),** 7092-7099.

[3] Soloff S, Adrian R, Liu Z C 1997 Distortion Compensation for generalised stereoscopic particle image velocimetry *Measurement Science and Technology*, (8), 1441-1454

[4] Qunot G, Rambert A, Lusseyran F, Gougat P 2001 Simple and accurate PIV camera calibration using a single target image and camera focal length *4th Int. Symp. Particle Image Velocimetry* (Gottingen: Germany), 1040.

[5] Fournel T, Lavest J M, Collange F 2003 Self-calibration of PIV video-cameras in Scheimpflug condition *Espagne: Springer*.

[6] Louhichi H, Fournel T, Lavest J M, Ben Aissia H 2007 Self-Calibration of Scheimpflug cameras: an easy protocol *Meas. Sci. Technol* 18 1-7.
[7] Lavest J M, Viala M, Dhome M 1998 Do we really need an accurate calibration pattern to acheive a reliable camera calibration In *Proc. of ECCV98,* (*Freiburg: Germany*), 158-174.
[8] Louhichi H, Fournel T, Lavest J, BenAissia H 2006 Camera selfcalibration in scheimpflug condition for air flow *investigation In proc of Advances in Visual Computing. Second International Symposium, ISVC, Part II , pp. 891 – 900, 2006.*
[9] Louhichi H, Fournel T, Lavest J, BenAissia H 2007 self-calibration of scheimpflug cameras: An easy protocol *Measurement Science and Technology, vol. 18, no. 8, pp. 2616 – 2622.*
[10] Haig C, Heipke C, Wiggenhagen M 2006 Lens inclination due to instable fixings detected and verified with vdi/vde *2634 part 1*.
[11] Wang J, Shi F, Zhang J, Liu Y 2008 A new calibration model of camera lens distortion *Pattern Recogn., vol. 41, no. 2, pp. 607–615.*
[12] Brown D 1966 Decentering distortion of lenses *vol. 32, no. 3, pp. 444–462.*
[13] Li J, Guo Y, Zhu J, Lin X, Xin Y, Duan K, Tang Q 2007 Large depth-of-view portable three-dimensional laser scanner and its segmental calibration for robot vision *Optics and Lasers in Engineering, vol. 45, pp. 1077 – 1087.*
[14] Legarda A, Izaguirre A, Arana N, Iturrospe A 2011 *International Workshop on Electronics, Control, Measurement and Signals - ECMS.*
[15] Fournel, T., Louhichi, H., Barat, C., Menudet, J.F.(2006). Scheimplug self-calibration based on tangency points. In *proc. of 12TH International Symposium of Flow Visualisation, (Göttingen, Germany).*